A Hybrid Firefly with Particle Swarm Optimization Based Hyperspectral Image Classification and Segmentation Using Structured Support Vector Machine

Manju Sundararajan[1*] , Sinthia Panneer Selvam[2] , Grace Shoba Samuel Jayachandran[1]

[1] Department of ECE, Velammal Engineering College, Surapet 600066, India
[2] Department of BME, Saveetha Engineering College, Thandalam 602105, India

Corresponding Author Email: manju.s@velammal.edu.in

ABSTRACT

Nowadays, hyperspectral satellite imaging (HSI) is widely being applied for terrain feature segmentation and classification in the remote sensing domain. However, such automated techniques for accurate segmentation and classification are still significant real-world challenges. To mitigate these challenges, a hybrid Firefly with Particle Swarm optimization (Hybrid FF with PSO) based hyperspectral satellite image segmentation and classification approach is proposed. This approach consists three major steps. At first, hyperspectral satellite images are pre-processed using the median filter to increase image quality and make categorization more efficient. Then, the input data is processed into a gray-level image, which serves as the matrix value for the image during the feature extraction process using a gray-level co-occurrence matrix (GLCM). These extracted images contain pixel values that have been improved classification results using a Hybrid FF with PSO approach. Then, HSI image is segmented using the binary classification procedure with the OTSU's threshold approach. At last, Structured Support Vector Machine (SSVM) with different image classes is used for the classification procedure. This research used datasets from AVIRIS sensor through a flight movement over the Indian pines location in North-western Indian. The simulation outcomes depict the proposed approach obtained superior performance than the conventional approaches in terms of sensitivity, specificity, accuracy, recall, precision, and F1-score.

1. INTRODUCTION

Many new use cases in remote sensing field and other areas of image investigation have become possible because of the increasing accessibility of hyperspectral data. Hyperspectral sensors simultaneously capture around 100 spectral bands (data channels). Therefore, the vector values related to the broad spectrum of reproduced light is given for every pixel in hyperspectral data [1]. For example, the Aerial Visible-Infrared Imaging Spectrometer (AVIRIS) device from NASA's Jet Propulsion Laboratory has 224 spectral channels with a spectral resolution of about 10 nm, reporting wavelengths from 0.4 to 2.5 meter [2]. The capacity to distinguish between structures and substances in the image is enhanced by the data's outstanding spectral determination, which contains a significant data source on the physical nature of the numerous resources. However, the high dimensionality of the data implied by the vast number of spectral channels makes image analysis and classification difficult. Most frequently applied techniques created for the study of grayscale, color, or multispectral images are ineffective for using HSI images. The availability of reference data is typically relatively low, impacting how well-supervised classification systems function. Also, the well-known "curse of dimensionality" for hyperspectral image analysis hinders

reliable statistical estimations, makes conventional vector norms useless, and more [3]. Thus, creating new algorithms is necessary to fully utilize the spectral dimension's rich information.

The initial categorizations for hyperspectral data had intended to categorize every pixel only based on its spectrum [4]. These methods for pixel-level processing use various data, including texture features, straight spectral information, and nonlinear and linear conversions of these features. The used feature extraction process frequently seeks to reduce the data dimensionality. There are various techniques used for image categorization based on its features such as neural networks [5, 6], kernel-based techniques [7, 8], Bayesian estimation approaches [9] and decision trees [10]. In general, support vector machines (SVM) and kernel-based techniques [11] depicts the better classification outcomes due to its robust when few training data is available.

In the image analysis, additional changes to enhances classification outcomes includes the mixing of spatial and spectral data. The determination of pixels to a particular class using feature vector its pixels data measured from its surrounding pixels. In conventional approaches, the spatial data involved in the categorization model based on Markove random fields [12] and morphological filters [13]. These approaches depict the better performance based on

classification accuracies. Moreover, these approaches use static window based nearby pixels. Image segmentation playing an important job to describe spatial structures using other approaches [14]. The areas attained from the segmentation describe the spatial information of the pixels inside these areas. Thus, an effective segmentation approach is required to achieve a robust image segmentation.

Hybridizing Firefly and PSO algorithms can leverage the exploration capabilities of PSO and exploitation capabilities of Firefly, achieving a balanced approach in exploring the hyperspectral feature space. However, this hybrid approach can lead to improved optimization helping to find both globally optimal and locally refined solutions in hyperspectral images classification compared with the latest deep learning models particularly Convolutional neural networks and Recurrent neural network.

Various approaches are introduced for hyperspectral image segmentation which utilize region integration methods in terms of spectral similarity. At first, each pixel is assumed as a distinct area and next pairs of areas are integrated using similarity of spectral and shape characteristics [15]. A hierarchical segmentation method used to make area growing and spectral grouping that established by Tilton [16]. The major disadvantages of using area integration for image segmentation is that the selection of similarity condition. These approaches result a pyramid of segmentation maps using a threshold which required manual analysis. Watershed transformation used to develop a statistical morphology-based segmentation method [17]. This method is indirect to segment multispectral images due to its multivariate pixels which need s numerical morphology. Multispectral segmentation based on numerical morphology is presented [18, 19] and watershed segmentation of color images are introduced [20].

A feature vector mean is created for each area using spectral-spatial classifier [21]. Initially, segmentation is achieved using area growing approach and feature vector mean is calculated for each area from the image which describes the average spectral data of each area pixels. Then, these areas are categorized using SVM classifier and the attained outcomes depict that there is no much improvement using pixel-wise classification. A spectral and spatial data classification of image is presented [22]. Also, a pixel-wise maximum likelihood and watershed segmentation is performed individually. The classification outcomes depict the considerable enhancement using spectral-spatial method than the pixel-wise maximum likelihood approach.

In this paper a hybrid approach can enhance feature selection by leveraging the ability of both firefly algorithm and particle swarm optimization to explore and exploit the feature space efficiently. This is crucial for selecting relevant spectral bands and discarding redundant or noisy information, leading to improved classification or analysis results. Hybrid approach can lead to better optimization of parameters in hyperspectral classification algorithms. This can result in improved accuracy in distinguishing different classes of hyperspectral images. In addition, the hybrid approach's adaptability allows it to handle the heterogeneity of hyperspectral pine images, enabling better optimization for diverse spectral characteristics.

The optimization strategy enhances the outcome using the particle swarm optimization algorithm by incorporating the binary threshold and gradient descent approach. It optimizes the space based on every particle's mobility to improve the outcome. This procedure creates PSOs with population values using movement of particle in the space which is adopted by the better progress of the swarm. Every particle's answer will be improved through iteration [23]. The PSO generates the binary image using OTSU's threshold function approach. The PSO generates the binary image using OTSU's threshold function approach for the image particles of the presented threshold area. A weighted and gradient function minimizes the error by creating a binary image. Since image segmentation uses this technique, remote sensing applications are used to optimize algorithms for supervised machine learning techniques.

2. RELATED WORK

K nearest neighbor (KNN) based spectral–spatial hyperspectral image categorization is presented [24]. This method, SVM is used for classification where the mapping of different classes is attained based on probability. Next, averaging nonlocal neighborhoods and matching is obtained for pixel-wise probability maps based KNN filtering approach. Then, the KNN approach is applied to use the original image's nonlocal principle fully, and sophisticated segmentation and optimization strategies weren't used in this method. This method uses two datasets and is compared with many classification results. A new method for creating segmentation benchmarks is presented and employed to develop hyperspectral training-test data segments ready for usage [25]. It can be used for better validation of both new and old techniques without leaking training or test data.

Resource-efficient quantized convolutional neural networks are presented and drastically reduce their size without degrading the capacity to classify data [26]. The tests using two hyperspectral benchmarks demonstrated that the quantization procedure can be used effectively while training, producing significantly smaller yet broadly applicable deep learning methods. The watershed segmentation technique is presented to segment hyperspectral data to determine spatial structure information [27]. The segmentation maps are subsequently included in a classifier, illuminating the accuracy of the watershed algorithms. Based on pixel-wise categorization using SVM, succeeded by majority voting within watershed areas, an original spectral-spatial categorization strategy for hyperspectral data is presented. The outcomes of investigational segmentation and classification on two hyperspectral data are exposed. Investigations have shown that feature extraction and multidimensional gradients are preferable to vectorial gradients as spectral bands rise. The classification accuracy is increased, and categorization maps with additional similar areas are produced due to the inclusion of spatial data from the watershed segmentation in the hyperspectral data clustering.

A unique method for unsupervised categorization of land cover use case utilizing multi-stage thresholding using the highest entropy to better the separation between objects and background [28]. A widely used segmentation tool is multi-level thresholding, which divides a gray-level image to numerous identical areas. The computing efficiency and robustness of the presented approach are enhanced by using Differential Evolution (DE), a popular and straightforward evolution process. By contrasting DE's performance with that of other well-known, environment-global optimization strategies, the effectiveness of DE is also thoroughly examined. The findings of the MRE-based thresholding were also applied to train an SVM classifier using a combined kernel technique

to increase the classification accuracy.

A multi-stage algorithm suitable for performing thematic categorization of hyperspectral satellite data using minimal training sets of data chosen from identified image sections is presented [29]. Without sensor condition data, this approach is necessary and is used relatively frequently in real-world situations. The technique of choice comprises the steps of pixel and spatially-based pre-processing, spatial post-processing of the categorization outcomes, and image categorization using spatial and spectral parameters. The trials revealed that the methodology based on merging pixel-level segmentation results from employing k-means, linked elements labeling, and nonlinear pre- and post-processing techniques produced the best outcomes.

A deep learning neural network is utilized in this study to determine techniques for satellite remote sensing data [30]. Before applying the image information to the segmentation step using a fuzzy-relevant vector machine, pre-processing is required. A Gaussian Filter approach based on Cellular Automata removes noise from satellite data. The pre-processed satellite data is next segmented utilizing the Fuzzy-Relevance vector machine Segmentation method to identify reverse shapes with the minimum energy. The recommended technique's results show an extraordinary accuracy of 98.9 percent compared to other techniques. The classification of hyperspectral images obtained from satellites is actualized in this work using a practical technique [31]. This approach is founded on enhancing SVM utilizing Self Organizing Maps (SOM). Then, inside and outside Picture element can be classified by comparing the Posterior Probability of every pixel intensity. This approach contains two steps, the initial step is to optimize the SVM utilizing self-organizing maps to extract the important characteristics from the image. The next step is determining the inside and outside pixels and associating the optimal threshold and probability. The presented methodology better than the traditional methods based on parameters such as, kappa, confusion matrix and accuracy.

To classify land cover, researchers provide a unique framework that accounts for the spectral and spatial image included in the data [32]. Employ the Gaussian Maximum Likelihood and CNN models for the pixel-by-pixel spectral categorization. Next, utilizing segmentation maps produced by the Watershed algorithm, integrate the spatial context data into this paper to use an altered maximum vote approach. The investigational evaluations on two standard datasets, the Pavia University and the Indian Pines datasets, show that recommended technique outperforms the existing techniques by reaching an accuracy of 99.52% and 98.31% on the corresponding datasets. A brand-new hyperspectral band selection method combines novel attention-based CNNs to weigh the bands [33]. The recommended attention-based method is data-driven, utilizes convolutional activations at various depths of a deep model, and identifies the spectrum's maximum valuable parts. Moreover, it can be trained using gradient descent from beginning to end and is modular, simple to use, and seamlessly transferable to any convolutional network. This approach testing, conducted across benchmark datasets and supported by statistical analyses, demonstrated that the deep systems with the consideration process are good with the traditional band selection methods.

The lightweight CNN method [34] considerably decreases computational costs by spreading spatial-spectral feature extraction over a lighter framework with pre-processing to enhance the classification performance. Five Hyperspectral benchmark datasets are employed for investigational estimation. The investigational outcomes demonstrate that the presented pipeline performed better than the traditional approaches regarding statistical significance, and computational complexity.

The proposed approach contains of two stages of hyperspectral image processing, including categorization and segmentation. The binary OTSU threshold approach is combined with the SSVM algorithm for classification. The Hybrid Firefly with Particle Swarm Optimization algorithm (Hybrid FF with PSO) uses the weighted function analysis. The image pixels are iteratively optimized using the modified optimization technique. We can increase the swarming variety based on the fitness value. The image's noise is reduced using the weighted least squares filter.

The workflow for the proposed approach, which includes the two primary methods of image classification and image segmentation, is shown in Figure 1. The SSVM technique is utilized to classify the images in this case. A HSI image dataset captured by an AVIRIS sensor makes up the input dataset. With its actual values, the Indian Pines dataset is applied for imaging techniques. This dataset is imported to obtain an image that has been transformed into binary form. With this binary image, threshold classification is performed. The weighted least squares (WLS) filter is applied to classify the image using the OTSU threshold approach. Now, we can determine the fitness value for each epoch using a Hybrid FF with PSO approach, which will decrease the computing cost. The segmentation of images uses the threshold method. Finding the ideal correlated value for image classification through principal component evaluation lowers the dimensionality and error rate of the images. It is applied to extract a limited collection of uncorrelated variables from a massive dataset of Indian pine.
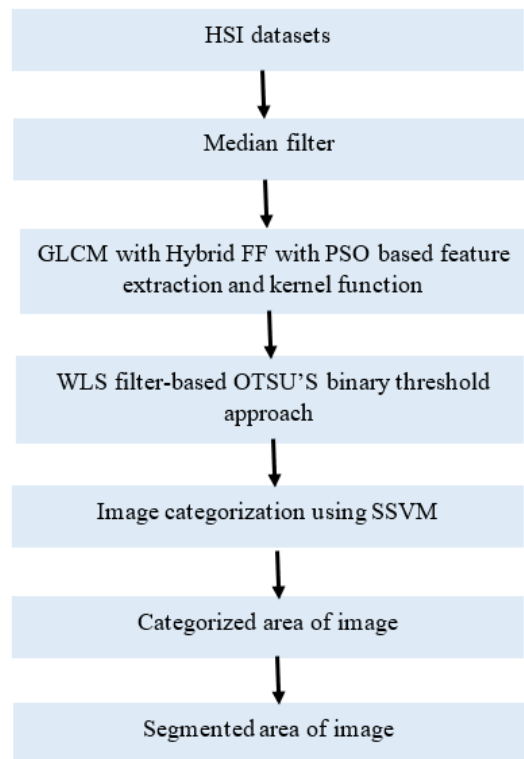

Figure 1. Proposed approach workflow

The hyperspectral satellite images are pre-processed using the median filter to increase image quality and make categorization more efficient. The input data is processed into a gray-level image, which serves as the matrix value for the image during the feature extraction process using GLCM. These extracted images contain pixel values that have been improved classification results using a Hybrid FF with PSO approach. The data is segmented in this case utilizing the binary categorization process by the OTSU's threshold model. The SSVM with different image classes is used for the classification procedure. The performance evaluation of proposed approach is obtained based on sensitivity, specificity, accuracy, recall, precision and F1-score once we have the train and test datasets from the SSVM. The proposed approach is compared to traditional approaches is enhanced the system performance.

2.1 Pre-processing using median filter

The median filter replaces the window's center value with the median of all the pixels, making it a sliding window spatial filter. Although this filter reduces noise, it loses fine details. Because median filters may effectively reduce many types of noise with less blurring, research frequently utilizes them. In addition to the signal, time series, and image processing, median filters are frequently employed as smoothers. The ability of the median filter to eradicate the effect of input noise with huge magnitudes is a significant advantage over linear filters. A non-linear filtering method that helps eliminate noise; the median filter has advantages over the mean filter. It can eliminate "impulse" noise (outlying values either high or low). Since step edges should be preserved without blurring, it was also frequently called "edge-preserving." Even though, it does slightly blur image edges when noise is present. The formula for the common median filter is Eq. (1), where A and B are the input and output, respectively, at position n of the filter. The $\{v_n\}_s$ s=1, ..., 2N+1, s^{th} order statistic of the datasets inside the window $\{v_n\}_1<\{v_n\}_2<\{v_n\}_3<\dots\{v_n\}2N+1$. The filters v_n is window size for this job, however, is 3×3. This size was chosen since rise in mask size will outcome in an increase in RMSE (Root Mean Square Error).

$$B_n=\text{med}\{V_n\}=\text{med}\{A_n+\text{s:s}\in V\} \quad (1)$$

2.2 GLCM feature extraction

Texture analysis has many uses, from texture categorization in remote sensing to biometric concerns to pattern identification in image retrieval. It is necessary to extract essential features that accomplish the texture features, which can be retrieved using GLCM to assist in extracting those features for each image processing procedure. GLCM, which has grown most common, is a statistical method for eliminating textural details from images. Hara lick defines fourteen textural features, measured from the probability matrix by the co-occurrence matrix, to extract the texture statistics of remote sensing images. The GLCM shows how frequently various sets of greyscale pixels appear in an image. It is produced for a particular pair of distance and angle. In Figure 2, relative recurrences are calculated for a given space and angle between every pixel and its neighbor.

This study recovers four significant characteristics: the Angular Second Moment, Inertia Moment, Correlation, Entropy, and Inverse Difference Moment.
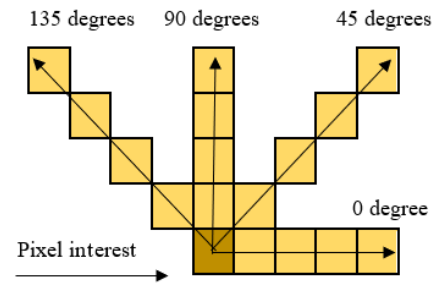
Figure 2. Pixel interest and it surrounding region for angle relative

2.2.1 Angular second moment

Another name for an Angular Second Moment (ASM) is uniformity or energy. It is the squared sum of all GLCM entries. The graphic similarity is measured by the ASM. When an image has excellent homogeneity or its pixels are substantially similar, the angular second moment is high. Eq. (2) is Gray tone is represented by k_g, where m and n are the spatial coordinates of the function $p(m, n)$.

$$\text{ASM}=\sum_{m=0}^{k_g-1} \sum_{n=0}^{k_g-1} Q_{mn}^2 \quad (2)$$

2.2.2 Inverse difference moment

Local similarity is defined as the inverse difference moment (IDM). This value is high when both the inverse GLCM and the local grey level are high. The value of the IDM weight is the opposite of the Contrast weight shows in Eq. (3).

$$\text{IDM}=\frac{\sum_{m=0}^{k_g-1} \sum_{n=0}^{k_g-1} Q_{mn}}{1+(n-m)^2} \quad (3)$$

2.2.3 Entropy

Entropy displays the amount of image information required for image compression. Entropy evaluates the image information and the data or message loss in a sent signal.

$$\text{Entropy}=\sum_{m=0}^{k_g-1} \sum_{n=0}^{k_g-1} Q_{mn}*\log Q_{mn} \quad (4)$$

2.2.4 Correlation

The linear association between the grey levels of nearby pixels is computed based on correlation. Image correlation is a visual approach that uses tracing and image registration approaches to quantify image modifies in 2D and 3D effectively. Widely utilized in many fields of science and engineering and is frequently applied to detect deformation, displacement, strain, and optical flow. Computing the motion of an optical mouse is one prevalent application.

$$\text{Correlation}=\frac{\sum_{m=0}^{k_g-1} \sum_{n=0}^{k_g-1} Q(m,n)-\mu_x \mu_y}{\sigma_x \sigma_y} \quad (5)$$

2.3 Hybrid FF with PSO approach

The brighter firefly always draws the less bright one in iterations of the firefly algorithm. This algorithm performs an excellent job of findings the answer in the random movement of the Neural Computing and Applications 123 location. Still, it ignores the firefly's ideal position and impacts how the problem is solved on a larger scale. The movement of fireflies

in Firefly Algorithm aims to explore the feature space efficiently, leading to the identification of relevant features for classification tasks. Mathematically, the movement of firefly i towards firefly j at iteration t+1 can be expressed as:

$$a_i(t+1) = a_i(t) + \beta e^{-\gamma r_{ij}^2}(a_j(t) - a_i(t)) + \alpha \varepsilon(t) \quad (6)$$

where, $a_i(t)$ is the position of firefly i at iteration t; r_{ij} is the distance between fireflies i and j; β is the attractiveness coefficient; γ is a constant; $\alpha\varepsilon(t)$ is a randomization term.
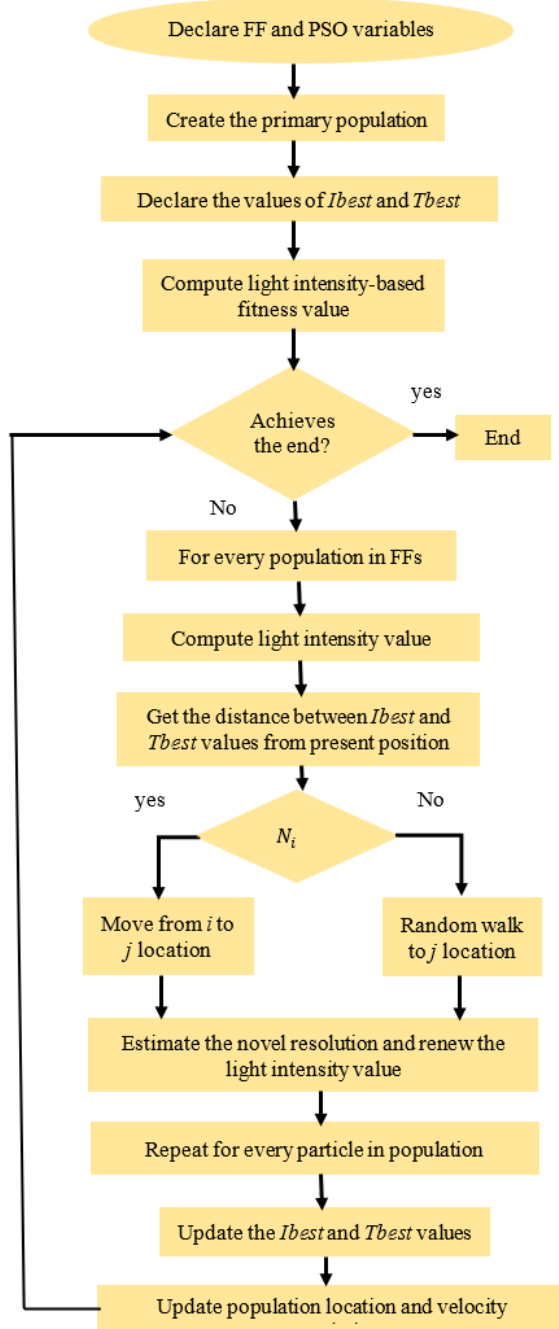

Figure 3. Hybrid FF with PSO algorithm flowchart

The drawback of specific PSO and FF algorithms are mitigated by hybrid approach of FF with PSO. In the global search space, the PSO algorithm discovers better solutions. The *Ibest* and *Tbest* numbers produced via PSO are utilized by every firefly. This method strikes a balance between exploitation and exploration to improve search results. Every

firefly's movement improves solution of accuracy and boosts convergence. Figure 3 shows the working process of hybrid FF with PSO optimization algorithm. The hybrid algorithm's position vector is provided by:

$$z_i^{l+1} = z_i^l + \mu_o e^{-\lambda r_{Iz}^2}(Ibest_i - z_i) +$$
$$\mu_o e^{-\lambda r_{Iz}^2}(Tbest_i) + \tau(\text{rand}-0.5) \quad (7)$$

where, *Ibest* is denote the Individual best position, *Tbest* is denotes the Total best position, μ is denotes Initial attractiveness, τ is denotes Randomized parameter, λ is denotes Light absorption coefficient.

The distance between z_i and *Ibest* is calculated using Euclidean distance. This can be described as:

$$r_{Iz} = \sqrt{\sum_{l=1}^{m}(best_{ij} - z_{ij})^2} \quad (8)$$

where, m is Number of populations.

The distance between z_i and *Tbest* is computed using Euclidean distance. This can be described as:

$$r_{Tz} = \sqrt{\sum_{l=1}^{m}(Tbest_{ij} - z_{ij})^2} \quad (9)$$

When an FF can't find an FF that is brighter than it, it randomly shifts positions in order to reach the global optimum.

$$z_i^{q+1} = z_i^q + \tau \varepsilon_i \quad (10)$$

where, q is denotes the Number of iterations.

2.4 Structured support vector machine is a machine learning (SSVM)

A Structured Support Vector Machine (SSVM) is a machine learning algorithm that extends the traditional support vector machine to handle structured output spaces. This is an approach that uses an SVM. for categorization of the HSI image is performed using the SSVM. The efficiency of the SSVM is enhanced through the optimization procedure. Regression, multiclass classification, and binary classification are the three basic concepts that employ this. Class labels are used in the train and test functions. After the network has processed test datasets, the datasets sent predicted using the training process. Here, the sources images are matched into respective labels using structured responses to produce complicated outcomes. The SSVM practices the kernel function for data transformations to find optimal results. The SSVM categorization logic is provided below:

$$d'(c; m) = sign\ (c, m) \quad (11)$$

$$d'(c; m) = sign\ (\rho(c, m)) \quad (12)$$

where, m is the weighted vector, c is an input array, $\rho(c)$ is the function of feature map, and d is output array. The regression equation given below:

$$H(Z) \sim (m,\ (\rho(c)) \quad (13)$$

In SSVM method, the relationship between input and output is mentioned below equation.

$$d'(c; m) = argmax\{m, \alpha\ (c,d)\}d \in D \quad (14)$$

Equation for regularization given below:

$$F(M) = \frac{\lambda}{2}\|m\|2 + 1/s \sum_{i=1}^{5} \Delta(d_i.d'(c_i;m)) \quad (15)$$

where, Δ is loss function, c_i is actual value of input and d_i is output. The pattern verification procedure attains the lesser space area in linear classification. The non-linear classification method is used for achieving a high dimensional area. Random array regularisation with high-dimensional data uses the Kernel function in this case. A process called "G" is used to denote the higher feature space, and it is provided in the equation:

$$G:c \rightarrow \varphi(c) \; \epsilon \quad (16)$$

2.5 OTSU's binary threshold approach

The structured output space defines the cost function during SSVM training. The testing procedure is processed using train datasets, which optimizes the outcome by choosing greater than zero values. The post-processing phase offers the categorized HSI image without an error signal.

Otsu's approach is a binary-valued image threshold technique. With this technique, grayscale images are transformed into binary images. The binary threshold method minimizes the intra-class variance, the weighted sum of variance with various classes.

$$\omega_m^2(s) = b_o(s)\omega_o^2(s) + b_1(s)\,\omega_1^2(s) \quad (17)$$

where, b_0 and b_1 is probability of each classes value, s is threshold factor, and ω_0^2 and ω_1^2 is variance of each classes value. The equations listed below estimate the histogram of these two classes.

$$b_o(s) = \sum_{i=0}^{s-1} r(i) \quad (18)$$

$$b_1(s) = \sum_{i=s}^{s-1} r(i) \quad (19)$$

Otsu's measurement procedure is implemented systematically with its respective classes. The algorithm first determines the variance's maximum and minimum values, determined by a threshold value, and the histogram's and every particle's probability. The intraclass interval is constrained to [-1, 1]. We can run an image threshold method based on the maximum variance of the classes.

3. RESULTS AND DISCUSSION

Indian pines are the source of the HSI dataset, which is gathered by the Airborne Visible Infra-Red Imaging Spectrometer (AVIRIS) sensor are used in this implementation. AVIRIS data is valuable for calibrating and validating models used in hyperspectral image classification. The extensive spectral information aids in refining the models to ensure accurate and reliable classification results. AVIRIS captures a large number of spectral bands in the visible and infrared regions. In addition, it provides both high spatial and spectral resolution. This may vary across different scenes, environments, and time points. The firefly algorithm's adaptability allows it to adjust its search strategy to the specific characteristics of the hyperspectral data, contributing to

improved robustness. The high spectral resolution facilitates the detection of subtle changes in the landscape. This is particularly useful for monitoring land cover dynamics, and assessing the impact of human activities on the environment.

This dataset is collected at test sites for Indian pines in northwest Indiana. There are 224 spectral bands and 145 pixels in this. This location has two-thirds agricultural land and one-third of forests or other types of natural vegetation. There are several classifications of land cover accessible with the actual data. Table 1 illustrates the Indian pines types with its samples.

Table 1. Indian pine types with samples

Number	Class	Samples
1	Stone-steel-towers	93
2	Alfalfa	46
3	Hay-windrowed	478
4	Corn-not	1428
5	Buildings-grass-trees-drives	386
6	Grass-pasture-mowed	28
7	Woods	1265
8	Grass tress	730
9	Oats	20
10	Corn-mintill	830
11	Wheat	205
12	Grass pasture	483
13	Soybean-clean	593
14	Soybean-mintill	2455
15	Corn	237
16	Soybean-notill	972

As a result, SSVM were used to model the categorization and segmentation of the HSI image, and Hybrid FF with PSO approach was used to optimize it. The SSVM approach is used to classify the images. With binary categorization, segmented images using Otsu's threshold method. Figure 4 depicts the input and grayscale image.

(a)   (b)
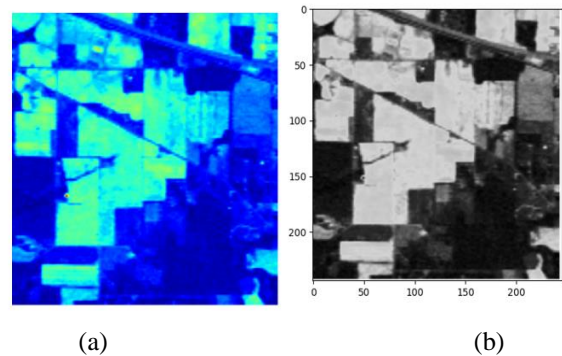
Figure 4. (a) Input image and (b) Grayscale image of (a)

(a)   (b)
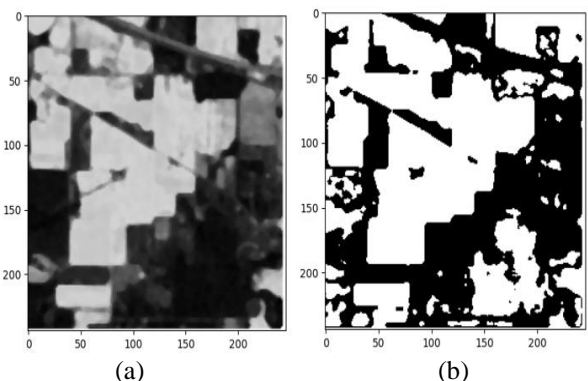
Figure 5. (a) Filtered image, (b) Otsu thresholding image

Table 2. OTSU Algorithm classification accuracy for the selected bands

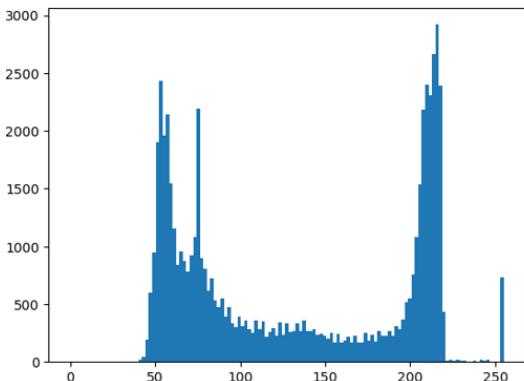| Class	10/Class	20/Class	30/Class	40/Class	50/Class	60/Class
Stone-steel-towers	89.91%	78.86%	86.45%	86.32%	96.23%	96.11%
Alfalfa	83.45%	86.12%	84.56%	87.94%	98.56%	96.23%
Hay-windrowed	86.00%	87.36%	86.32%	84.57%	86.93%	85.67%
Corn-not	87.23%	89.32%	85.56%	84.23%	87.23%	87.66%
Buildings-grass-trees-drives	76.54%	45.65%	96.23%	54.58%	96.32%	87.56%
Grass-pasture-mowed	49.56%	23.54%	94.26%	96.24%	56.23%	65.23%
Woods	81.23%	89.36%	86.59%	96.23%	95.84%	65.89%
Grass tress	56.24%	78.96%	82.32%	97.86%	85.64%	89.32%
Oats	87.12%	75.63%	84.57%	96.23%	95.14%	95.12%
Corn-mintill	91.02%	74.23%	86.29%	86.23%	95.36%	86.22%
Wheat	85.63%	87.59%	81.02%	84.26%	94.63%	85.23%
Grass pasture	87.24%	86.49%	83.21%	78.94%	86.95%	89.23%
Soybean-clean	86.00%	82.15%	86.30%	76.59%	83.26%	87.56%
Soybean-mintill	87.32%	88.98%	84.36%	91.23%	87.32%	87.66%
Corn	87.45%	85.63%	89.65%	87.56%	87.21%	86.21%
Soybean-notill	89.91%	78.86%	86.45%	86.32%	96.23%	96.11%
Average	81.46	77.32	86.51	85.93	88.86	86.06

The binary threshold method, which segments the image into several classes of regions, is used for image segmentation. Figure 5 (a) shows that the filtered image using median filtering and (b) The segmented hyperspectral image by binary threshold approach.

Otsu Thresholding is performed to select highly informative band from 224 spectral bands. A set of six training samples is randomly picked with reference to ground truth labels from selected bands on each execution to study the selected bands. The samples are 10, 20, 30, 40, 50, 60 taken per each class to justify OTSU algorithm classification accuracy Table 2 depicts the OTSU algorithm classification accuracy of AVIRIS Indian Pine classes.
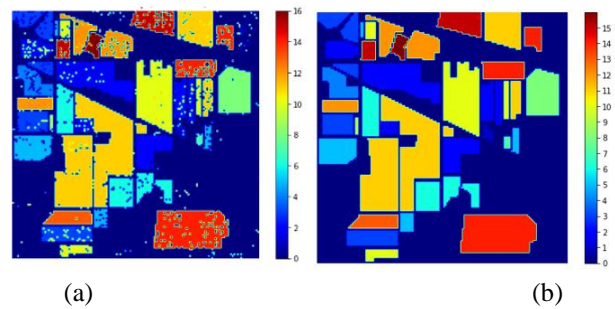
The selected bands are used for classification. The SSVM-Hybrid FF with PSO technique is used to classify the HSI image of the Indian Pines. Four-band spectrum models are used to represent several classification zones. With the help of a SSVM, 16 types are trained and tested. WLS filter is performed in the thresholding procedure to filter the categorized image. Figure 6 illustrates how WLS filters reduce errors in hyperspectral images.

Figure 7 (a) depicts the classification outcome of proposed SSVM- Hybrid FF-PSO approach and (b) depicts the ground truth image classification of Indian pines.

A classification algorithm's performance is evaluated using a table called a confusion matrix. The outcome of a classification algorithm is shown and summarized in a confusion matrix. Table 3 is showing the confusion matrix.


(a)   (b)

Figure 7. (a) Classification of SSVM – Hybrid FF-PSO, (b) ground truth image classification of Indian pines

Table 3. Confusion matrix

Actual value	Predicted Value	
	True Positive (TP)	False Negative (FN)
	False Positive (FP)	True Negative (TN)

Sensitivity, specificity, accuracy, recall, precision and F1-score are extracted from the confusion matrix variables such as, TP, FN, FP, and TN.

Figure 6. WLS filter-based error reduction
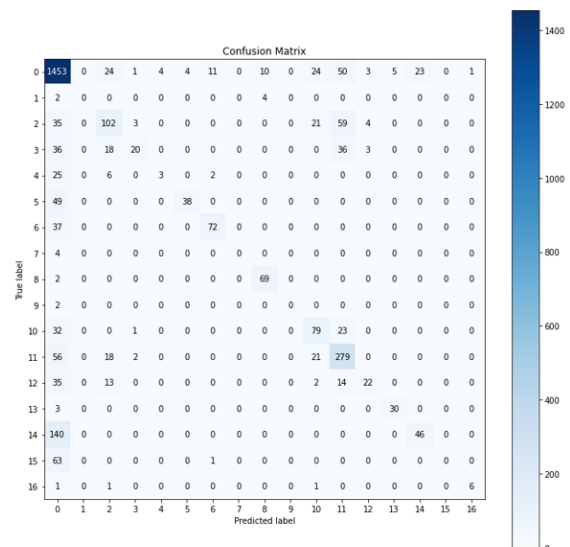
Figure 8. Confusion matrix of proposed approach

1523

Figure 8 illustrates the confusion matrix of the proposed technique which describes the Y axis denotes the true label, while the X axis denotes the predicted label. Analysing the rows, it illustrates that the approach classified quite accurately. Also, it provides the details of classification findings for Indian pines, split into 16 types.

The system's effectiveness evaluates how precisely vegetated land is divided into 16 types. Sensitivity evaluates the 16-types vegetated land's positive classification rate when the state is genuinely present, called the false-negative rate.

$$Sensitivity = \frac{True\ Positive(TP)}{True\ Positive(TP) + False\ Negative(FN)} \quad (20)$$

When the requirement is genuinely absent, specificity evaluates the 16-type vegetation land's classification in the negative. A false-positive rate is used to illustrate it.

$$Specificity = \frac{True\ Negative(TN)}{True\ Negative(TN) + False\ Positive(FP)} \quad (21)$$

The following equation is applied to calculate the accuracy of the proposed approaches.

$$Accuracy = \frac{True\ Positive(TP) + True\ Negative(TN)}{True\ positive(TP) + True\ Negative(TN) + False\ Positive(FP) + False\ Negative(FN)} \quad (22)$$

Recall computes how many exact class estimates are produced using all of the successful cases in the database.

$$Recall = \frac{True\ Positive(TP)}{True\ Positive(TP) + False\ Negative(FN)} \quad (23)$$

The amount of positive classes estimates that truly fall within the positive class is measured by precision.

$$Precision = \frac{Precision\ x\ Recall}{Precision + Recall} \quad (24)$$

F-Measure offers a single score that compromises recall and precision requirements.

$$F1\text{-}Score = 2\ x\ \frac{True\ Positive(TP)}{True\ Positive(TP) + False\ Negative(FN)} \quad (25)$$

Table 4 demonstrates the performance of the proposed and existing approaches sensitivity, specificity, and accuracy comparison table. In Relevance vector machine (RVM) the optimization process involves iterative updates, and the sparsity -inducing priors can lead to non-convex optimization problems. And so, RVM results in a more complex model with a small number of support vectors. In order to improve the high dimensionality feature selection Improved Relevance vector machine with Mosquito Flying Algorithm is applied. However, the accuracy is very less compared with the proposed approach. The accuracy with extreme learning machine classifier (ELM) is also performed and found to be less than hybrid approach. The fixed random weights in the input to hidden layer connections can limit the model capacity to capture the high dimensional features. It is also compared with dragon fly algorithm (DF) where each particle in the optimization corresponds to possible solution in the search space. Its performance may degrade in high dimensional space and hence the accuracy of 70% is achieved. Upon comparison with all the methods hybrid approach proved to be significant approach.

Table 4. Performance comparison of proposed approach

Approaches	Sensitivity	Specificity	Accuracy
Proposed approach	94	98	81.43
IRVM-MFO	10	94.06	50.8
ELM	31.75	68.95	49.88
DF-ELM	70	90	70

Table 5. Proposed approach results of recall, precision, and F1-score

Parameter	Value
Recall	76.29
Precision	80.36
F1- Score	88.56
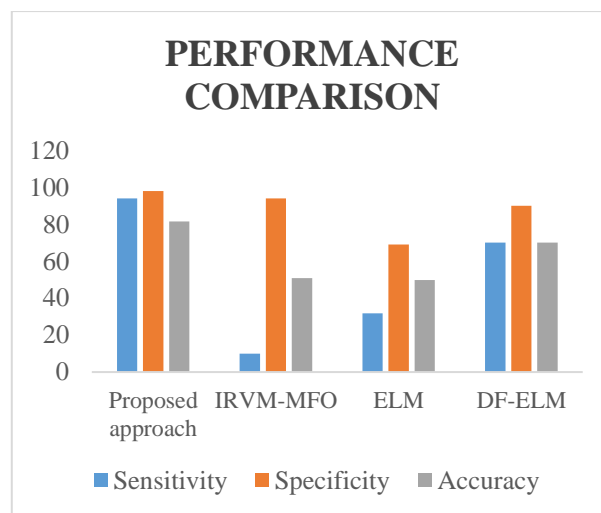
Figure 9. Performance comparison of proposed approach

Figure 9 shows the performance comparison of SSVM-Hybrid FF-PSO classification and conventional approaches in terms of sensitivity, specificity, and accuracy. The proposed approach achieved better outcomes than other conventional approaches.
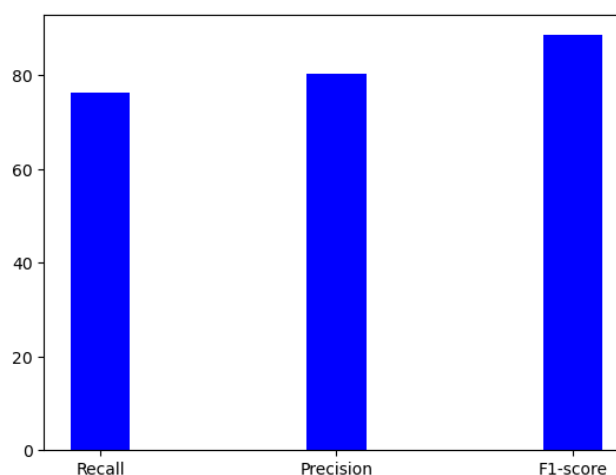
Figure 10. Recall, precision, and F1-score of Proposed approach results

Table 5 and Figure 10 depict the performance of proposed Hybrid FF with PSO based SSVM attained better recall, precision and F1-score.

4. CONCLUSIONS

This work analyzed the optimized SSVM for the HSI image for segmentation and categorization based on Hybrid FF with PSO strategy and Otsu's binary threshold categorization technique is presented. The input dataset consists of an area of Indian pines detected using Airborne Hyper-Spectral Infrared Imaging Spectroscopy. Here, the pre-processing phase of the SSVM uses the median filter, and the post-processing step uses the weighted least square filter, both of which will diminish the error and image noise before and after categorization. With Otsu's binary threshold categorization approach, GLCM is applied in the segmented process. As a result, the hyperspectral image was categorized and segmented using the suggested SSVM- Hybrid FF with PSO approach. Compared to other procedures, this produces superior outcomes. The test and train function in SSVM is used to evaluate several classification areas and achieved 94% of sensitivity, 98% of specificity, 81.43% of accuracy, 76.29% of recall, 80.36% of precision, and 88.56% of F1-score. This approach produces superior outcomes than other traditional approaches. In the future, this research work taken to the further classification with selected bands and combining SSVM with reinforcement learning techniques to improve the classification accuracy better.

REFERENCES

[1] Plaza, A., Benediktsson, J.A., Boardman, J.W., Brazile, J., Bruzzone, L., Camps-Valls, G., Trianni, G. (2009). Recent advances in techniques for hyperspectral image processing. Remote Sensing of Environment, 113: S110-S122. https://doi.org/10.1016/j.rse.2007.07.028

[2] Moussaoui, S., Hauksdottir, H., Schmidt, F., Jutten, C., Chanussot, J., Brie, D., Douté, S., Benediktsson, J.A. (2008). On the decomposition of Mars hyperspectral data by ICA and Bayesian positive source separation. Neurocomputing, 71(10-12): 2194-2208. https://doi.org/10.1016/j.neucom.2007.07.034

[3] Osma-Ruiz, V., Godino-Llorente, J.I., Sáenz-Lechón, N., Gómez-Vilda, P. (2007). An improved watershed algorithm based on efficient computation of shortest paths. Pattern Recognition, 40(3): 1078-1090. https://doi.org/10.1016/j.patcog.2006.06.025

[4] Chen, Y., Lin, Z., Zhao, X., Wang, G., Gu, Y. (2014). Deep learning-based classification of hyperspectral data. IEEE Journal of Selected Topics in Applied Earth Observations and Remote Sensing, 7(6): 2094-2107. https://doi.org/10.1109/JSTARS.2014.2329330

[5] Goel, P.K., Prasher, S.O., Patel, R.M., Landry, J.A., Bonnell, R.B., Viau, A.A. (2003). Classification of hyperspectral data by decision trees and artificial neural networks to identify weed stress and nitrogen status of corn. Computers and Electronics in Agriculture, 39(2): 67-93. https://doi.org/10.1016/S0168-1699(03)00020-6

[6] Chen, C.H., Ho, P.G.P. (2008). Statistical pattern recognition in remote sensing. Pattern Recognition, 41(9): 2731-2741. https://doi.org/10.1016/j.patcog.2008.04.013

[7] Landgrebe, D.A. (2003). Signal Theory Methods in Multispectral Remote Sensing (Vol. 24). John Wiley & Sons.

[8] Bali, N., Mohammad-Djafari, A. (2008). Bayesian approach with hidden Markov modeling and mean field approximation for hyperspectral data analysis. IEEE Transactions on Image Processing, 17(2): 217-225. https://doi.org/10.1109/TIP.2007.914227

[9] Aptoula, E., Lefèvre, S. (2007). A comparative study on multivariate mathematical morphology. Pattern Recognition, 40(11): 2914-2929. https://doi.org/10.1016/j.patcog.2007.02.004

[10] Chang, C.I. (2003). Hyperspectral Imaging: Techniques for Spectral Detection and Classification. Springer Science & Business Media.

[11] Melgani, F., Bruzzone, L. (2004). Classification of hyperspectral remote sensing images with support vector machines. IEEE Transactions on Geoscience and Remote Sensing, 42(8): 1778-1790. https://doi.org/10.1109/TGRS.2004.831865

[12] Zhou, H., Mao, Z., Wang, D. (2005). Classification of coastal areas by airborne hyperspectral image. In Proceedings Volume 5832, Optical Technologies for Atmospheric, Ocean, and Environmental Studies, pp. 471-476. https://doi.org/10.1117/12.619684

[13] Bali, N., Mohammad-Djafari, A. (2008). Bayesian approach with hidden Markov modeling and mean field approximation for hyperspectral data analysis. IEEE Transactions on Image Processing, 17(2): 217-225. https://doi.org/10.1109/TIP.2007.914227

[14] Chen, S., Zhang, D. (2004). Robust image segmentation using FCM with spatial constraints based on new kernel-induced distance measure. IEEE Transactions on Systems, Man, and Cybernetics, Part B (Cybernetics), 34(4): 1907-1916. https://doi.org/10.1109/TSMCB.2004.831165

[15] Fauvel, M., Chanussot, J., Benediktsson, J.A. (2006). Evaluation of kernels for multiclass classification of hyperspectral remote sensing data. In 2006 IEEE International Conference on Acoustics Speech and Signal Processing Proceedings, Toulouse, France, pp. II-II. https://doi.org/10.1109/ICASSP.2006.1660467

[16] Guo, B., Gunn, S.R., Damper, R.I., Nelson, J.D. (2008). Customizing kernel functions for SVM-based hyperspectral image classification. IEEE Transactions on Image Processing, 17(4): 622-629. https://doi.org/10.1109/TIP.2008.918955

[17] Yi, F., Moon, I., Javidi, B. (2016). Cell morphology-based classification of red blood cells using holographic imaging informatics. Biomedical Optics Express, 7(6): 2385-2399. https://doi.org/10.1364/BOE.7.002385

[18] Hanbury, A.G., Serra, J. (2001). Morphological operators on the unit circle. IEEE Transactions on Image Processing, 10(12): 1842-1850. https://doi.org/10.1109/83.974569

[19] Lambert, P., Chanussot, J. (2000). Extending mathematical morphology to color image processing. In International Conference on Color in Graphics and Image Processing - CGIP'2000, pp. 158-163.

[20] Angulo, J., Serra, J. (2003). Mathematical morphology in color spaces applied to the analysis of cartographic images. Proceedings of GEOPRO, 3: 59-66.

[21] Van der Linden, S., Janz, A., Waske, B., Eiden, M., Hostert, P. (2007). Classifying segmented hyperspectral data from a heterogeneous urban environment using support vector machines. Journal of Applied Remote Sensing, 1(1): 013543. https://doi.org/10.1117/1.2813466

[22] Li, P., Xiao, X. (2004). Evaluation of multiscale morphological segmentation of multispectral imagery for land cover classification. In 2004 IEEE International Geoscience and Remote Sensing Symposium, Anchorage, AK, USA, pp. 2676-2679. https://doi.org/10.1109/IGARSS.2004.1369851

[23] Chen, X., Zhan, S., Ji, D., Xu, L., Wu, C., Li, X. (2023). Image denoising via deep network based on edge enhancement. Journal of Ambient Intelligence and Humanized Computing, 14(11): 14795-14805. https://doi.org/10.1007/s12652-018-1036-4

[24] Huang, K., Li, S., Kang, X., Fang, L. (2016). Spectral–spatial hyperspectral image classification based on KNN. Sensing and Imaging, 17: 1-13. https://doi.org/10.1007/s11220-015-0126-z

[25] Nalepa, J., Myller, M., Kawulok, M. (2019). Validating hyperspectral image segmentation. IEEE Geoscience and Remote Sensing Letters, 16(8): 1264-1268. https://doi.org/10.1109/LGRS.2019.2895697

[26] Nalepa, J., Antoniak, M., Myller, M., Lorenzo, P.R., Marcinkiewicz, M. (2020). Towards resource-frugal deep convolutional neural networks for hyperspectral image segmentation. Microprocessors and Microsystems, 73: 102994. https://doi.org/10.1016/j.micpro.2020.102994

[27] Tarabalka, Y., Chanussot, J., Benediktsson, J.A. (2010). Segmentation and classification of hyperspectral images using watershed transformation. Pattern Recognition, 43(7): 2367-2379. https://doi.org/10.1016/j.patcog.2010.01.016

[28] Sarkar, S., Das, S., Chaudhuri, S.S. (2016). Hyper-spectral image segmentation using Rényi entropy based multi-level thresholding aided with differential evolution. Expert Systems with Applications, 50: 120-129. https://doi.org/10.1016/j.eswa.2015.11.016

[29] Fedoseev, V.A. (2018). Hyperspectral satellite image classification using small training data from its samples. Journal of Physics: Conference Series, 1096(1): 012042. https://doi.org/10.1088/1742-6596/1096/1/012042

[30] Vinuja, G., Devi, N.B. (2023). Multitemporal hyperspectral satellite image analysis and classification using fast scale invariant feature transform and deep learning neural network classifier. Earth Science Informatics, 16(1): 877-886. https://doi.org/10.1007/s12145-023-00948-2

[31] Jain, D.K., Dubey, S.B., Choubey, R.K., Sinhal, A., Arjaria, S.K., Jain, A., Wang, H. (2018). An approach for hyperspectral image classification by optimizing SVM using self-organizing map. Journal of Computational Science, 25: 252-259. https://doi.org/10.1016/j.jocs.2017.07.016

[32] Gupta, S.T., Sahay, S.K. (2020). A Novel Spatial-Spectral Framework for the Classification of Hyperspectral Satellite Imagery. In Proceedings of the 21st EANN (Engineering Applications of Neural Networks) 2020 Conference, pp. 227-239. https://doi.org/10.1007/978-3-030-48791-1_17

[33] Lorenzo, P.R., Tulczyjew, L., Marcinkiewicz, M., Nalepa, J. (2020). Hyperspectral band selection using attention-based convolutional neural networks. IEEE Access, 8: 42384-42403. https://doi.org/10.1109/ACCESS.2020.2977454

[34] Ahmad, M., Shabbir, S., Raza, R.A., Mazzara, M., Distefano, S., Khan, A.M. (2021). Hyperspectral image classification: Artifacts of dimension reduction on hybrid CNN. arXiv preprint arXiv:2101.10532. https://doi.org/10.48550/arXiv.2101.10532